A Simple Photonics-Based Measurement Method for Microwave DFS and AOA

Qianqian Jia, Jinye Li, Liangchen Sun, Dechen Li, and Jianguo Liu, *Member, IEEE*

***Abstract*—This article put forwards a simple microwave photonics measurement method for microwave doppler frequency shift (DFS) and angle of arrival (AOA), which obtains the information conveniently and precisely by comparing the frequency and phase shift between two channels signals. The DFS direction can be judged more intuitively thanks to the introduction of the reference signal. The system uses two parallel dual parallel Mach-Zehnder modulators (DPMZMs) for carrier suppression single-sideband (CS-SSB) modulation. A proof-of-concept experiment was taken, showing that during ±100 kHz, the DFS measurement error is <±0.1 Hz over a 40 GHz frequency range as well as power sensitivity is down to −50 dBm. What is more, the measurement error of AOA is < ±1° from 0° to 90°. This simple system acquits excellent width band performance without the optical filter, providing a reliable and more conducive to human-computer interaction solution for future measurement and sensing applications.**

***Index Terms*—Angle of arrival, doppler frequency shift, microwave photonics.**

I. Introduction

DURING intelligent driving, radar detection, wireless communication, internet of things and other emerging fields, it is critical to determine the real-time location of moving objects [1]–[2], which involves doppler frequency shift (DFS) as well as angle of arrival (AOA) measurements [3]–[6]. DFS is the frequency shift between the back and come signals [7], and is applied to obtain the velocity of the object. The angle of the moving target can be estimated by AOA, which can be calculated through the phase difference between the echoes received by spatially-separated antennas [1]–[7]. However, the narrow bandwidth and poor stability of key electronic devices limit the application of traditional electrical systems. Nowadays, photonics-based methods have attracted great attentions due to the excellent quality of large instantaneous bandwidth, high robustness, and low transmission loss [8]–[13].

So far, a series of photonics systems to measure DFS [14]–[20] or AOA [21]–[25] have emerged. For example, [20] uses a parallel dual parallel Mach-Zehnder modulators (DPMZM) combing reference signal to measure DFS. The point of this method is combing the transmitted, as well as the reference signals together forming one signal for direction judgment. In addition, [25] uses two Mach-Zehnder modulators (MZMs) to measure phase shifts between transmitted and echo signals and calculates AOA via obtaining the optical powers of the two branches. However, as far as we know, many reported systems are used for measurement of either DFS or AOA, which limits the application of the systems and hard to fast obtain and the accurate location of the subject. To solve this problem, some photonics systems [2]–[3], [7], [26]–[28] have been proposed in the past 3 years.

In 2019, Peng Li [26] firstly proposed a photonic method using for long range antenna to measure both two parameters, including a polarization-division-multiplexed Mach-Zehnder modulator (PDM-MZM) and a phase modulator (PM). The frequency and phase difference between two channels are measured to obtain DFS (including direction) and AOA. Experimental results reveal that the DFS measurement error is $< \pm 5\times10^{-3}$ Hz during ±100 kHz, as well as the AOA error is <0.85° from 1.82° to 90° at 10 GHz and <2.25° from 4.35° to 90° at 18 GHz. Unfortunately, this system cannot identify the DFS direction when the target moves along the perpendicular bisector of the two receive antennas. In the same year, Zhenzhou Tang [3] designed a microwave photonics-based scheme to simultaneously measure both two parameters for automotive radars, including parallel MZM and polarization-division-multiplexed MZM(PDM-MZM). This system can obtain DFS (with direction identification) and AOA by using the optical hybrid, consisting of two orthogonal outputs. The DFS error is <2.5 Hz in ±100 kHz and the AOA error is < ±2.3°from 27.25° to 90°. However, both two systems are complex for using two I/Q dual channels or tunable optical filter. Next year, Chongjia Huang [27] proposed a simpler system consisting of only one optical modulator. Experimental results show that when the transmitted signal is around 15 GHz, the DFS error is < ±0.2 Hz, and the AOA error is < ±1°from 0° to 90°. However, this system needs to strictly control the working state such as carrier–suppression ratio, phase balance, and working point of modulators. In 2021, dual channels simple system was put forward [28], showing that

Manuscript received March 28, 2022; revised May 6, 2022; accepted May 18, 2022. Date of publication May 30, 2022; date of current version June 3, 2022. This work was supported by the National Natural Science Foundation of China under Grant 61727815. *(Qianqian jia, Jinye Li, and Liangchen Sun contributed equally to this work). (Corresponding author: Jianguo Liu.)*

Qianqian Jia and Jianguo Liu are with the Institute of Semiconductors, Chinese Academy of Sciences, Beijing 100083, China, and also with the Center of Materials Science and Optoelectronics Engineering, University of Chinese Academy of Sciences, Beijing 100049, China (e-mail: jiaqianqian@semi.ac.cn; jgliu@semi.ac.cn).

Jinye Li is with the Institute of Semiconductors, Chinese Academy of Sciences, Beijing 100083, China (e-mail: jyli@semi.ac.cn).

Liangchen Sun and Dechen Li are with the Institute of Semiconductors, Chinese Academy of Sciences, Beijing 100083, China, and also with the College of Electronic, Electrical and Communication Engineering, University of Chinese Academy of Sciences, Beijing 100049, China (e-mail: sunliangchen@semi.ac.cn; lidechen@semi.ac.cn).

Digital Object Identifier 10.1109/JPHOT.2022.3177194

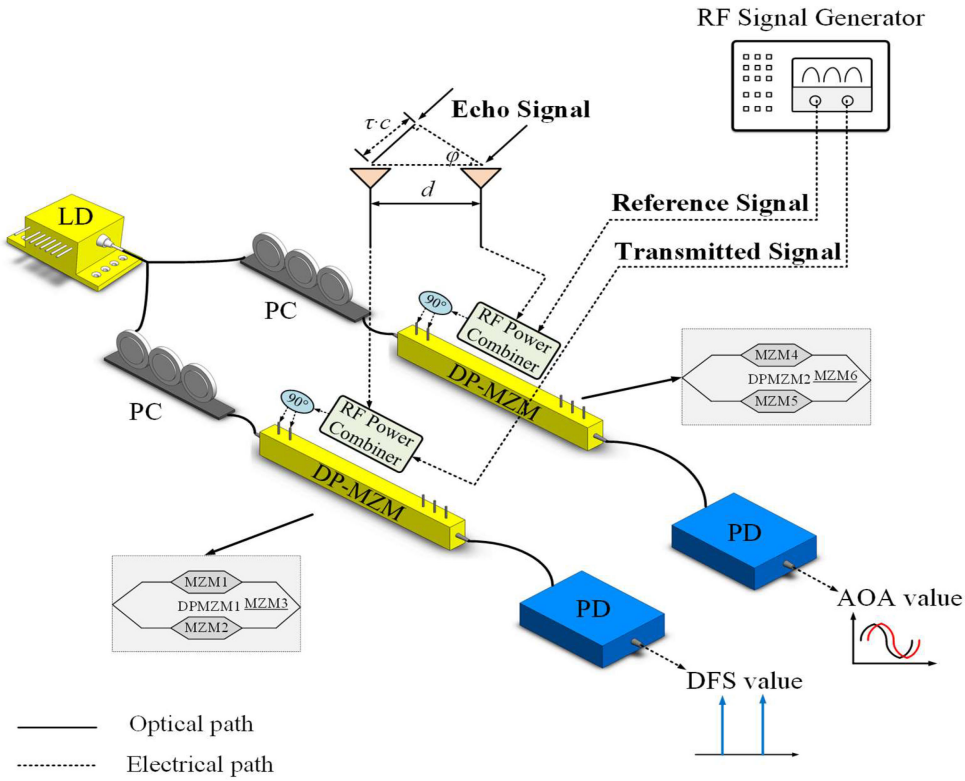

Fig. 1. Schematic diagram of the proposed measurement method. LD: Laser diode; PC: Polarization controller; MZM: Mach-Zehnder modulator; DPMZM: Dual parallel Mach–Zehnder modulator; PD: Photodiode.

during ±100 kHz, the DFS measurement error is $< \pm 0.08$ Hz, and from 0° to 90°, the AOA error is $< \pm 1.3°$. However, there still exists the problem of unintuitive display of DFS results or the system bandwidth limitation for using optical bandpass filter.

In this article, a simple microwave photonics system to measure DFS and AOA is proposed, which obtains the information by comparing the frequency value and phase shift of two channels' down-converted signals, and because of the introduction of the reference signal, the DFS's direction can be judged more intuitively. In this system, transmitted, echo and reference signals are loaded into two DPMZMs to implement carrier suppression single-sideband (CS-SSB) signal modulation, separately. As a result, the DFS (including values and direction) and AOA can be gotten from the two branches by comparing the value and phase difference between two IF down-converted signals. It is obvious that the DFS results can be displayed visually by using the reference signal. What's more, CS-SSB modulation can make full use of spectrum resources without using optical filters, expand system operating bandwidth, and simplify system configuration.

II. Principle

As shown in Fig. 1, followed by two polarization controllers (PC), a laser diode (LD) is divided into two paths, which is described as:

$$E(t) = E_0 e^{j\omega_c t} \tag{1}$$

where E_0 is amplitude as well as ω_c is the angular frequency of LD. Then two continuous wave (CW) lights are injected into two parallel DPMZMs, the upper and lower. While the upper DPMZM1 is a composition of three MZMs, one parent MZM (MZM3) and two sub-MZMs (MZM1 and MZM2). Three bias voltages, V_{bias1}, V_{bias2} and V_{bias3} control the working state of the upper DPMZM1. Like DPMZM1, DPMZM2 also consists of three MZMs, where three bias voltages, V_{bias4}, V_{bias5}, and V_{bias6} control the working state of DPMZM2, similarly.

In the proposed system, three kinds of signals, a reference (Rx), a transmitted (Tx), and two echo (EX1 and EX2) are introduced, which can be described as:

$$\begin{aligned} RX(t) &= V_r \cos(\omega_r t + \alpha) \\ TX(t) &= V_t \cos(\omega_t t) \\ EX1(t) &= V_e \cos(\omega_e t) \\ EX2(t) &= V_e \cos(\omega_e t + \theta) \end{aligned} \tag{2}$$

where V_{r} and ω_{r} are the reference signal' amplitude and angular frequency, respectively. Similarly, V_{t} and ω_{t} are the transmitted signal' amplitude and angular frequency, and V_{e} and ω_{e} are the echo signals' amplitude and angular frequency. α is the initial phase of the reference signal. AOA is related to the two received echo signals' phase difference θ, which can be calculated by:

$$\begin{aligned} \theta &= \omega_e \tau + 2k\pi \\ \varphi &= \cos^{-1}\left(\frac{c\tau}{d}\right) \end{aligned} \tag{3}$$

where τ, d, c, and φ are the relative time delay between two echo signals, two antennas' distance, the light speed, and the AOA of two echo signals, which are also illustrated in Fig. 1.

An electrical combiner (EC) is used to combine the reference signal and one of the echo signals. After that, the combined one is divided into two quadrature signals through an electrical 90-degree bridge and injected into DPMZM1 to implement the CS-SSB modulation, whose output optical field is derived as:

$$\begin{aligned} &E_{upper}(t) \\ &= \frac{E(t)}{\sqrt{2}} \cos\left(\frac{\varphi_{DC1}+\beta_r \cos(\omega_r t+\alpha)+\beta_e \cos(\omega_e t+\theta)}{2}\right) \\ &\quad + \frac{\exp(j\theta_3)\, E(t)}{\sqrt{2}} \\ &\quad \times \cos\left(\frac{\varphi_{DC2}+\beta_r \sin(\omega_r t+\alpha)+\beta_e \sin(\omega_e t+\theta)}{2}\right) \end{aligned} \tag{4}$$

where β is the modulation depth of MZMs, $\varphi_{\mathrm{DC1}} = \pi V_{\mathrm{bias1}}/V_\pi$ and $\varphi_{\mathrm{DC2}} = \pi V_{\mathrm{bias1}}/V_\pi$ are the optical phases introduced by V_{bias1} of MZM1 and V_{bias2} of MZM2, as well as V_π is MZMs' half-wave voltage. Besides, $\theta_3 = V_{\mathrm{bias3}}/V_\pi$, is the phase introduced by MZM3 of DPMZM1. When MZM1 and MZM2 are set at the null points and MZM3 is set at the quadrature point ($\varphi_{\mathrm{DC1}} = \pi$, $\varphi_{\mathrm{DC2}} = \pi$, $\theta_3 = \pi/2$), CS-SSB modulation is generated. Here, the higher order sidebands ($\geq$2) are ignored, and the DPMZM1's output optical field is derived as:

$$E_{MZM1}(t) \propto \frac{E(t)}{2} \left\{ \begin{array}{l} J_1(m_r)\sin(\omega_r t+\alpha) \\ +J_1(m_e)\sin(\omega_e t+\theta) \\ +J_{-1}(m_r)\sin(-\omega_r t-\alpha) \\ +J_{-1}(m_e)\sin(-\omega_e t-\theta) \end{array} \right\} \tag{5}$$

$$E_{MZM2}(t) \propto \frac{E(t)}{2} \left\{ \begin{array}{l} J_1(m_r)\cos(\omega_r t+\alpha) \\ +J_1(m_e)\cos(\omega_e t+\theta) \\ +J_{-1}(m_r)\cos(-\omega_r t-\alpha) \\ +J_{-1}(m_e)\cos(-\omega_e t-\theta) \end{array} \right\} \tag{6}$$

$$E_{upper}(t) = \frac{E(t)}{\sqrt{2}} \left\{ \begin{array}{l} J_{-1}(m_r)\sin(-\omega_r t-\alpha) \\ +J_{-1}(m_e)\sin(-\omega_e t-\theta) \end{array} \right\} \tag{7}$$

where $\mathrm{J}_{\pm\mathrm{n}}()$ is the $\pm$nst first kind Bessel function. $m_r = \pi V_r/V_\pi$, $m_e = \pi V_\mathrm{e}/V_\pi$ are the reference and echo signals' modulation indexes.

On the other hand, the transmitted signal and the other echo signal are coupled by an EC and loaded on the lower DPMZM2, and the output optical field is described as:

$$\begin{aligned} E_{lower}(t) &= \frac{E(t)}{\sqrt{2}} \cos\left(\frac{\varphi_{DC4}+\beta_t \cos(\omega_t t)+\beta_e \cos(\omega_e t)}{2}\right) \\ &\quad + \frac{E(t)\exp(j\theta_6)}{\sqrt{2}} \\ &\quad \times \cos\left(\frac{\varphi_{DC5}+\beta_t \sin(\omega_t t)+\beta_e \sin(\omega_e t)}{2}\right) \end{aligned} \tag{8}$$

where $\varphi_{\mathrm{DC4}} = \pi V_{\mathrm{bias4}}/V_\pi$, $\varphi_{\mathrm{DC5}} = \pi V_{\mathrm{bias5}}/V_\pi$, and $\theta_6 = V_{\mathrm{bias6}}/V_\pi$ are the optical phases introduced by V_{bias4} of MZM4, V_{bias5} of MZM5, and V_{bias6} of MZM6. V_π is MZMs' half-wave voltage. Similarly, by setting $\varphi_{\mathrm{DC4}} = \pi$, $\varphi_{\mathrm{DC5}} = \pi$, $\theta_6 = \pi/2$, the lower DPMZM2 also works in CS-SSB situation. Considering the condition of small-signal approximation, the DPMZM2's output optical field is written as:

$$E_{lower}(t) = \frac{E(t)}{\sqrt{2}} \left\{ \begin{array}{l} J_{-1}(m_t)\sin(-\omega_t t) \\ +J_{-1}(m_e)\sin(-\omega_e t) \end{array} \right\} \tag{9}$$

where $m_t = \pi V_\mathrm{t}/V_\pi$ is the modulation index of the transmitted signal. Then two branches' optical signals are sent to two low-speed PDs for beat frequency processing to eliminate high frequency spurs as much as possible, obtaining two down-converted IF signals, which are written as:

$$\begin{aligned} I_{upper}(t) &\propto \eta {E_0}^2 \{J_{-1}(m_t) J_{-1}(m_e) \\ &\qquad \times \cos[(\omega_\mathrm{e}-\omega_\mathrm{r})t+\theta-\alpha]\} \\ I_{lower}(t) &\propto \eta {E_0}^2 \{J_{-1}(m_r) J_{-1}(m_e)\cos[(\omega_e-\omega_t)t]\} \end{aligned} \tag{10}$$

where η is the responsivity of PDs. When $\omega_\mathrm{t} \neq \omega_\mathrm{r}$, the value of DFS can be gotten in the lower branch, at the same time, the direction of DFS can be also gotten by comparing the frequencies between the two branches. Moreover, when $\theta = 0°$, the DFS direction can also be identified. Thanks to the reference signal, the DFS direction can be clearly judged by numerical comparison.

For example, the spectral relationship of difference signals is shown in Fig. 2 (assuming that the reference signal is larger than the transmitted signal). When f_r-f_e>f_r-f_t as shown in Fig. 2(a), the DFS is negative and the object is far away from the radar. Similarly, when f_e-f_t>f_r-f_t, the DFS is positive and the echo signal is on the right of the reference signal in Fig. 2(b); when f_e-f_t<f_r-f_t and f_e-f_r<f_r-f_t, the echo signal is between the reference and transmitted signals in Fig. 2(c).

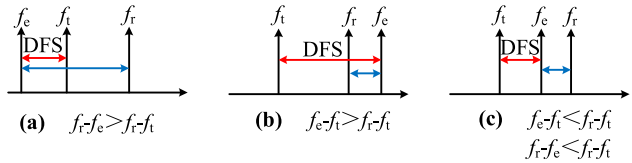

Fig. 2. The spectral relationship of the difference signals of various echo, transmitted, and reference signals.

When $\omega_\mathrm{t} = \omega_\mathrm{r}$, the (10) can be written as (11) shown at the bottom of the this page.

$$\left\{ \begin{array}{l} I_{upper}(t) \propto \eta {E_0}^2 \{J_{-1}(m_r) J_{-1}(m_e)\cos[(\omega_\mathrm{e}-\omega_t)t+\theta-\alpha]\} \\ I_{lower}(t) \propto \eta {E_0}^2 \{J_{-1}(m_t) J_{-1}(m_e)\cos[(\omega_e-\omega_t)t]\} \end{array} \right. , \omega_\mathrm{e} > \omega_t$$
$$\left\{ \begin{array}{l} I_{upper}(t) \propto \eta {E_0}^2 \{J_{-1}(m_r) J_{-1}(m_e)\cos[(\omega_t-\omega_e)t+\alpha-\theta]\} \\ I_{lower}(t) \propto \eta {E_0}^2 \{J_{-1}(m_t) J_{-1}(m_e)\cos[(\omega_t-\omega_e)t]\} \end{array} \right. , \omega_\mathrm{e} < \omega_t \tag{11}$$

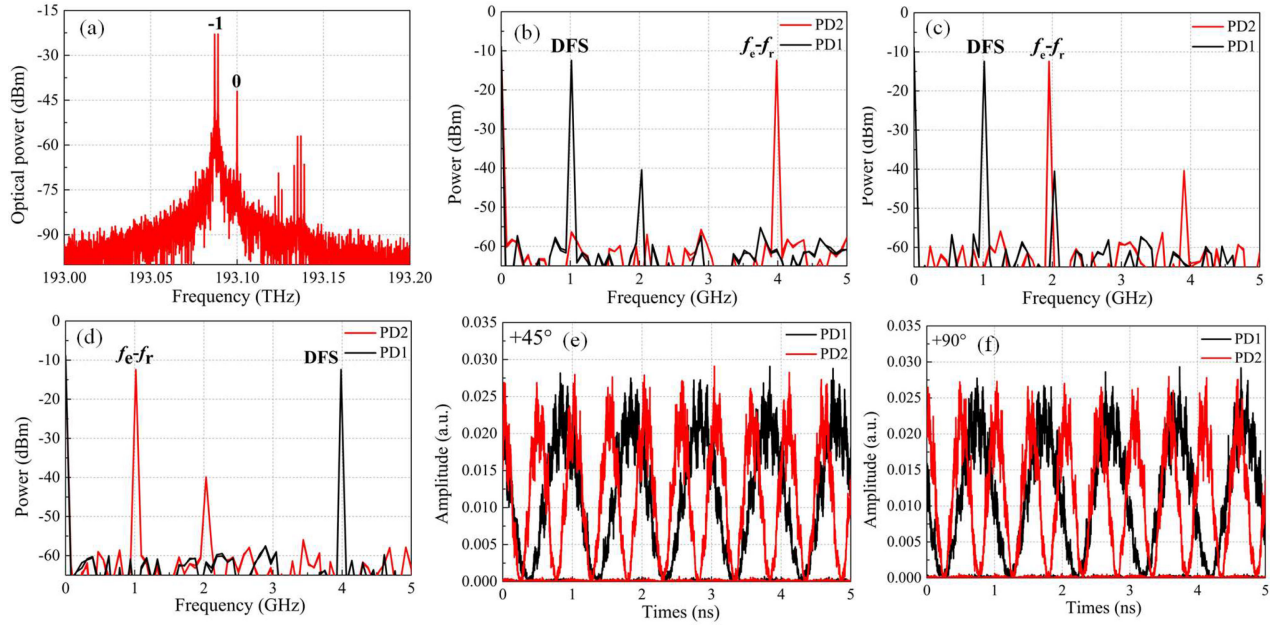

Fig. 3. Simulation results of the proposed system by OptiSystem. The CS-SSB modulation signals' spectrum of echo, transmitted and reference signals is (a); when $f_t = 13$ GHz, $f_r = 10$ GHz, the electrical spectra of various echo signals ($f_e = 11$ GHz, 9 GHz, 14 GHz) are (b)-(d); When $f_r = 13$ GHz, $f_t = 10$ GHz, $f_e = 11$ GHz with $\theta = 45°$ or 90°, electrical waveforms of two PDs are (e)-(f).

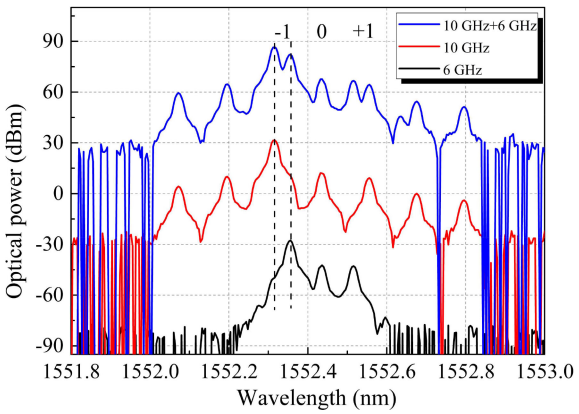

Fig. 4. The optical spectra of one or two modulated signals.

Similarly, the value of DFS can be gotten in the either branch. The direction of DFS and the value of AOA can be obtained from the phase difference between the two branches. Assuming $0<\theta<\alpha$, when the waveform of the upper branch is ahead of the lower, the DFS is negative; when the waveform of the upper branch is behind the lower, the DFS is positive. In addition, the AOA value can be calculated by comparing the phase difference between two branches. More importantly, the method can judge the DFS direction even when $\theta = 0°$. The introduction of the reference signal is convenient for judging the direction of the DFS, making the measurement more convenient and intuitive.

III. Experimental Setup and Results

A. Simulation and Experimental Setup

In this chapter, the simulation and experimental analysis of the system are completed. Based on the system design in Fig. 1, the simulation results by Opti System are summarized in Fig. 3. Fig. 3(a) illustrates optical spectra of two DPMZMs, showing that the echo, transmitted, and reference signals are all modulated in CS-SSB situation. When $f_r = 13$ GHz and $f_t = 10$ GHz with the same initial phases, the electrical spectra of various echo signals ($f_e = 9$ GHz, 11 GHz, 14 GHz) are exhibited in Fig. 3(b)–(d). It is obvious that the numerical comparison between two IF signals is related to the DFS direction. By comparing the phase shift between two branches, the value of AOA can be easily gotten as shown in Fig. 3(e) and (f). When $f_r = 13$ GHz, $f_t = 10$ GHz, and $f_e = 11$ GHz, the two the phase difference of two IF signals are compared and calculated as 45° (Fig. 3(e)) and 90° (Fig. 3(f)). According to (3), the AOA value is calculated by combining other parameters of the echo antennas.

Next, the proposed simple system is experimentally tested and analyzed. The LD with 1550.012 nm center wavelength, an average power of 10 dBm, a 10 MHz linewidth, and a maximum relative intensity noise of −150 dB/Hz is divided into two branches and launches into two parallel DPMZM (MXIQER-LN-30) via two PCs. In this experiment, transmitted, reference, and echo signals are generated by three microwave signal generators (MSGs). Furthermore, the power of three kinds of signals is 15 dBm, 15 dBm, and 0 dBm to simulate real test conditions as closely as possible, and the working situation of DPMZMs is controlled by the bias control electrical board.

In the upper branch, the reference signal and one of the echo signals are generated from MSGs (E8257D and N5166B), and coupled with an electrical combiner (RS2W10400-K) and applied to drive DPMZM1 with 40 GHz, an insertion loss of 6 dB and a 4 V half-wave voltage after passing an electrical 90-degree bridge (TBG-20400-3K-90) to implement CS-SSB modulation following by the EDFA to enlarge the signal. Like the upper

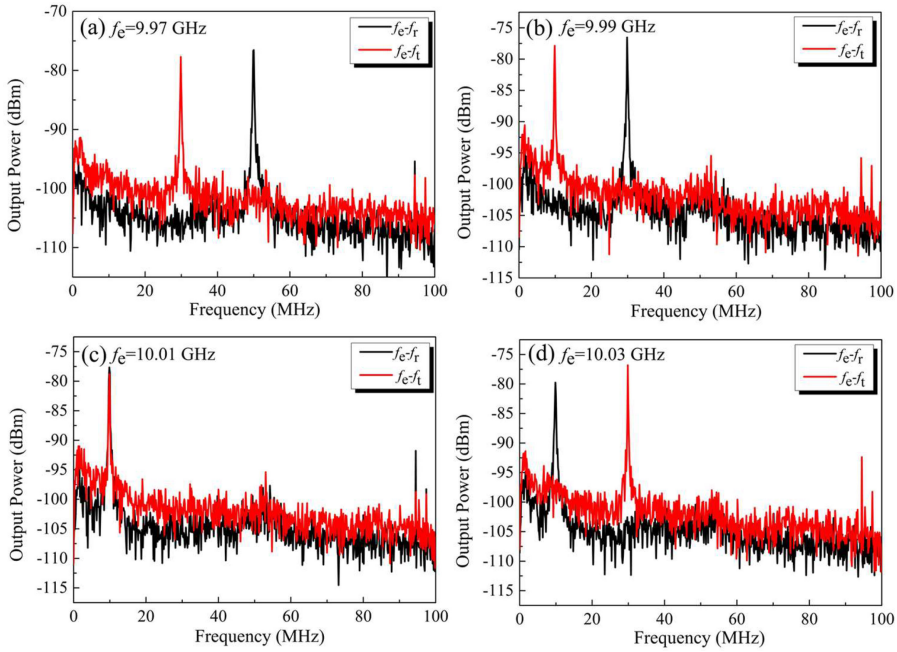

Fig. 5. The electrical spectra of DFS measurement with different echo signals.

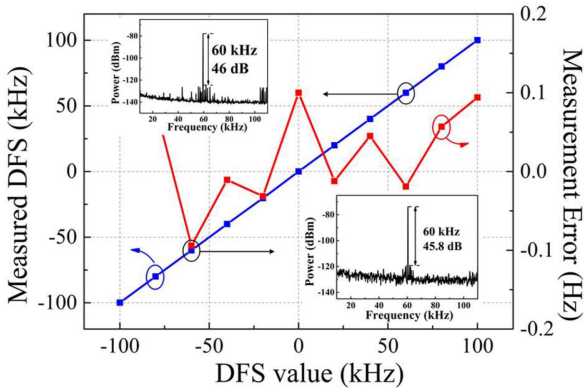

Fig. 6. The DFS measurement results and errors, when $f_t = 5$ GHz.

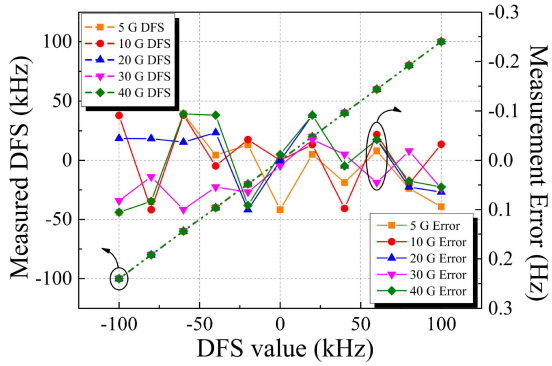

Fig. 7. The DFS measurement results (dash lines) and errors (solid lines), with the transmitted signal of 5, 10, 20, 30, and 40 GHz.

branches, the transmitted, and the other echo signals are injected into the lower DPMZM2. After CS-SSB modulation, two branches are injected into two low-speed PDs (DET01CFC/M) with a bandwidth of 2 GHz, and the down-converted beating signals are processed by a real-time oscilloscope (DSAZ594A) to measure the two parameters. In the experiment, an optical spectrum analyzer (AQ6370D) is used to measure the optical spectrum and an electrical signal analyzer (ESA) (FSV-40) is used to observe the electrical spectrum, which operates with a 50 Hz resolution bandwidth (RBW) and 3 kHz video bandwidth (VBW).

Fig. 4 shows the modulated signals' optical spectra. When the RF signal is 6 GHz (black line) or 10 GHz (red line), the output optical field of DPMZM is CS-SSB modulation. Similarly, two RF signals of 10 GHz and 6 GHz are coupled and injected into

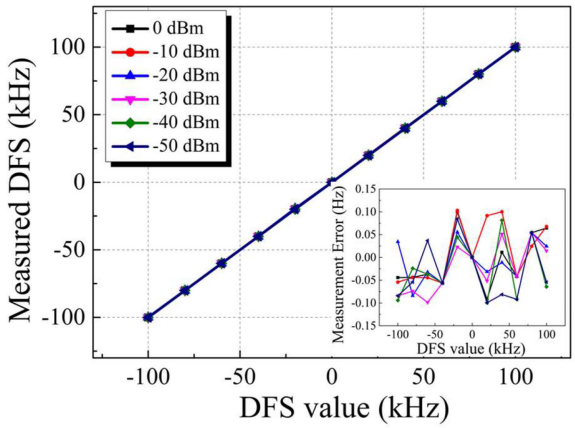

Fig. 8. The DFS measurement results and errors, with the power of echo signals of 0, −10, −20, −30, −40, and −50 dBm.

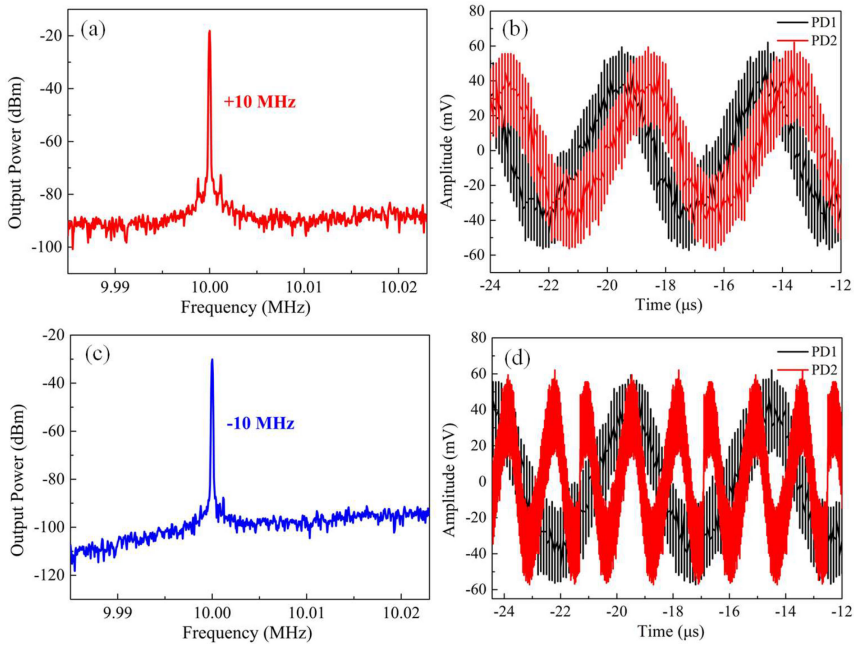

Fig. 9. Electrical waveforms (b), (d) and (a), (c) Spectra of down-converted IF signals when $f_e = 10.01$ GHz or 9.99 GHz.

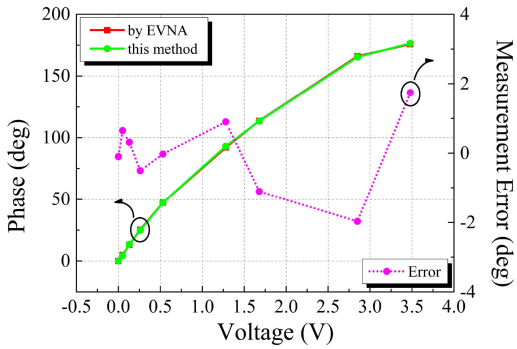

Fig. 10. AOA and errors measured by VNA and the proposed system at 15 GHz.

DPMZM, and the CS-SSB modulation is implemented with the optical carrier is more than 15 dB lower than the remained -1st-order sideband.

B. DFS Measurement

To judge DFS direction, when $f_r = 10.02$ GHz and $f_t = 10$ GHz, the measured electrical spectra of various echo signals are exhibited in Fig. 5, showing the simulation results are in good agreement with the experiments. When the echo signals are 9.99 GHz or 10.01 GHz, the DFS is equal to 10 MHz, as shown in Fig. 5(b) and (c), while it is difficult to judge the DFS direction at this time. However, the introduction of the reference signal solves this problem. By comparing f_r-f_e, the direction of DFS can be easily gotten. Similarly, when the echo signals are 9.97 GHz or 10.03 GHz, the DFS is equal to 30 MHz, as shown in Fig. 5(a) and (d) and the different f_r-f_e helps to distinguish the DFS direction. In general, the introduction of reference frequency can assist in measuring any value of DFS and accurately determine the DFS direction, which has application potential in practical measurement systems.

Next, a series of different transmitted and echo signals are sited to measure DFS and analyze errors. When $f_t = 5$ GHz, echo signals are changed from 4.99999 to 5.00001 GHz whose step size is 10 kHz, and the DFS is measured by ESA operating with a 1 Hz RBW and 1 Hz VBW in Fig. 6. The experimental results perform good consistency with theoretical simulations, showing that the error is less than $\pm$0.1 Hz. In addition, the electrical spectra with a DFS of $\pm$60 kHz are shown in Fig. 6 as insets.

What's more, by changing the transmitted signal frequency to measure DFS and errors, the operating bandwidth and performance of the simple system can be analyzed. For example, when the transmitted signal is 5,10,20,30, and 40 GHz, the DFS during $\pm$100 kHz is measured and measurement errors are exhibited in Fig. 7, showing that the errors with broadband frequencies are $<\pm$ 0.1 Hz. In addition, since echo signals' power received by the antenna is weak in the actual measurement environment, the sensitivity of the measurement system is also a concern. As a result, when the transmitted signal is fixed at 15 GHz with 0 dBm, the power of echo signals is changed from 0 dBm to -50 dBm whose step size is 10 dBm, and the DFS measurement results and errors are summarized in Fig. 8. Similarly, the measurement errors are less than $\pm$ 0.1 Hz over wideband frequencies without using optical filters. Furthermore, the use of a lower noise laser, amplifier or PDs can increase the sensitivity of microwave photonics link [29]–[30].

C. AOA Measurement

As shown in Fig. 9, the electrical waveforms, and spectra of the two branches are measured. When $f_r = 10.02$ GHz, $f_t = 10$ GHz with the same initial phases, and $f_e = 10.01$ GHz, the DFS is

TABLE I
PERFORMANCE COMPARISON BETWEEN THE PROPOSED METHOD AND THE PREVIOUSLY REPORTED SYSTEMS

Ref.	[26]	[3]	[27]	[7]	[28]	This work
Maximum Carrier Frequency	10 GHz	10 GHz	15 GHz	15 GHz	40 GHz	40 GHz
Range of AOA Measurements	0°-180°	0°-160°	0°-90°	0°-360°	0°-180°	0°-180°
Measurement Errors DFS and AOA	±0.005 Hz < 0.85°(1.82°-90°)	±2.5 Hz < 2.3°(27.25°-90°)	±0.2 Hz < 1°(0°-90°)	±0.07 Hz < 3.4°(±0°-±90°)	±0.08 Hz < 1.3°(0°-90°)	±0.1 Hz < 1°(0°-90°)
Identification of DFS Direction (When θ = 0°)	×	√	×	√	√	√
Minimum Power of Echo Signal	/	/	/	/	-90 dBm	-50 dBm
Key Devices of System	PM+PDM-MZM+TOF+2PDs	MZM+PDM-MZM+2OBPFs+90°Hybrids+2BPDs	DP-DDMZM+OF+PD	DPMZM+WDM+2PDs	PDM-MZM+OBPF+2PDs	2DPMZMs+2PDs

10 MHz with positive direction as shown in Fig. 9(a). Similarly, when $f_e = 9.99$ GHz, the DFS is 10 MHz with negative direction as shown in Fig. 9(c). One electrical 90-degree bridge is used to introduce phase shift between two echo signals. Fig. 9(b) and (d) exhibit curve variation relationship of beat frequency signals of two branches, which is consistent with the DFS direction. When DFS is positive, the phase difference between the two signals is 90 degrees, and when DFS is negative, the phase difference between the two signals is -90 degrees. The phase difference measurement error of the two branches down-converted IF signals are related to the system state. For example, the offset point drift of the modulators and the asymmetry of the two signals, etc. will introduce additional phase difference, thus affecting the accuracy of the final measurement results. On the other hand, keeping the transmitted equaling reference signals as well as the phase of two echo signals same, the distance between the two branches curves shows phase difference introduced by other environmental factors, which can be used to improve AOA measurement accuracy.

Furthermore, when $f_r = 15.002$ GHz and $f_t = 15$ GHz with the same initial phases, a voltage-controlled microwave phase shifter (CVPS-8G18G-360) is used to induce a variable phase difference θ of two echo signals as 15.001 GHz. As shown in Fig. 10, the measurement of phase shifts both by vector network analyzer (VNA) and the proposed method are compared, revealing that from 0° to 180°, the error is $<\pm 1.9°$. According to (3), the AOA errors are calculated as $<\pm 1°$from 0° to 90°. When the frequencies of the reference signal and the transmitted signal are different and two branches beat signals are different, the initial position of the waveform is usually difficult to determine during practical applications. Therefore, the reference signal and the transmit signal are set to the same frequency, which is convenient for actual measurement.

D. Discussion

As a result, sufficient theoretical simulation analysis and experimental results reveal that the proposed DFS and AOA measurement method has high measurement accuracy and wide operating bandwidth. Comparing the reported works with the method proposed in this paper, as shown in Table I, the proposed method has the advantages of simple structure, high measurement accuracy and sensitivity. For example, [27] presents a simple fiber link consisting of a LD, an optical modulator, an optical filter, and a PD. Unlike other methods, this scheme uses the frequency and power of a low-frequency electrical signal output by only one PD to calculate DFS and AOA, which has a simple structure, a large operating bandwidth, and good robustness. However, this scheme cannot judge the direction of DFS when $\theta = 0°$, and the introduction of a tunable optical filter limits the operating bandwidth of the system during actual measurement. Compared with the former, the proposed system uses two optical modulators and has an extensive working bandwidth without optical filter. What's more, the introduction of the reference signal is more convenient to determine the DFS direction, more conducive to human-computer interaction, which can be used in more situations. To sum up, the proposed scheme calculates DFS and AOA by comparing two low-frequency signals, which is more intuitive and convenient. In addition, compared with other two-signal schemes, the introduction of a reference signal makes it is easier to judge the direction of DFS even when $\theta = 0°$ by the comparison with the frequency and phase shift of two branches, which improves the measurement accuracy and is conducive to human-computer interaction. More importantly, the solution does not need filters resulting in a large measurement bandwidth, and can be integrated on-chip.

IV. CONCLUSION

As a result, a simple microwave photonics measurement system is proposed for DFS and AOA, which obtains the microwave DFS and AOA information by comparing the frequency and phase shift of two channels' down-converted signals. Thanks to the reference signal, the DFS direction can be judged more intuitively even when $\theta = 0°$. A proof-of-concept experiment shows that DFS measurement error during ± 100 kHz is $<\pm$ 0.1 Hz, the power of echo signals measurement accuracy is -50 dBm and the AOA measurement error is $<\pm 1°$from 0° to 90°. Furthermore, the measurement system works over wideband and

performs the simple structure and on-chip integration possibilities without the optical filter. The proposed system provides a reliable and more conducive to human-computer interaction solution for future measurement and sensing applications.

REFERENCES

[1] H. Chen, C. Huang, and E. H. W. Chan, "Photonic approach for measuring AOA of multiple signals with improved measurement accuracy," *IEEE Photon. J.*, vol. 12, no. 3, Jun. 2020, Art no. 7201810.

[2] X. H. Cao, X. J. Fan, G. Y. Li, M. Li, N. H. Zhu, and W. Li, "A filterless photonic approach for DFS and AOA measurement using a push-pull DPol-MZM," *IEEE Photon. Technol. Lett.*, vol. 34, no. 1, pp. 19–22, Jan. 2022.

[3] Z. Tang and S. Pan, "Simultaneous measurement of Doppler-frequency-shift and angle-of-arrival of microwave signals for automotive radars," in *Proc. Int. Topical Meeting Microw. Photon.*, 2019, pp. 1–4.

[4] Z. Tian, C. Ye, and Y. Jin, "Device-free indoor tracking via joint estimation of DFS and AoA using CSI amplitude," in *Proc. Int. Conf. Microw. Millimeter Wave Technol.*, 2021, pp. 1–3.

[5] P. Ghelfi *et al.*, "A fully photonics-based coherent radar system," *Nature*, vol. 507, no. 7492, pp. 341–345, 2014.

[6] G. Li *et al.*, "Unambiguous measurement of AOA using a DDMZM," *Opt. Commun.*, vol. 514, 2022, Art. no. 128132.

[7] H. Zhuo and A. Wen, "A photonic approach for Doppler-frequency-shift and angle-of-arrival measurement without direction ambiguity," *J. Lightw. Technol.*, vol. 39, no. 6, pp. 1688–1695, 2020.

[8] J. Zhang and J. Li, "Microwave photonics," in *Satellite Photoelectric Sensing Technology*. Cham, Switzerland: Springer, 2022, pp. 11–30.

[9] J. Capmany and D. Novak, "Microwave photonics combines two worlds," *Nature Photon.*, vol. 1, no. 6, pp. 319–330, 2007.

[10] J. P. Yao, "Microwave photonics," *J. Lightw. Technol.*, vol. 27, no. 3, pp. 314–335, 2009.

[11] Y. Zi *et al.*, "Optical injection locking assisted all-optical microwave oscillator," *Opt. Commun.*, vol. 509, 2022, Art. no. 127859.

[12] S. Pan and J. Yao, "Photonics-based broadband microwave measurement," *J. Lightw. Technol.*, vol. 35, no. 16, pp. 3498–3513, 2017.

[13] R. A. Minasian, E. H. W. Chan, and X. Yi, "Microwave photonic signal processing," *Opt. Exp.*, vol. 21, no. 19, pp. 22918–22936, 2013.

[14] W. Chen *et al.*, "Wideband Doppler frequency shift measurement and direction discrimination based on a DPMZM," *IEEE Photon. J.*, vol. 9, no. 2, Apr. 2017, Art no. 5501008.

[15] X. Zou, W. Li, B. Lu, W. Pan, L. Yan, and L. Shao, "Photonic approach to wide-frequency range high resolution microwave/millimeter-wave Doppler frequency shift estimation," *IEEE Trans. Microw. Theory Tech.*, vol. 63, no. 4, pp. 1421–1430, Apr. 2015.

[16] B. Lu, W. Pan, X. Zou, X. Yan, L. Yan, and B. Luo, "Wideband Doppler frequency shift measurement and direction ambiguity resolution using optical frequency shift and optical heterodyning," *Opt. Lett.*, vol. 40, no. 10, pp. 2321–2324, 2015.

[17] L. Xu, Y. Yu, H. Tang, and X. Zhang, "A simplified photonic approach to measuring the microwave Doppler frequency shift," *IEEE Photon. Technol. Lett.*, vol. 30, no. 3, pp. 246–249, Feb. 2018.

[18] Y. Gao *et al.*, "A simple and all-optical microwave Doppler frequency shift and phase measurement system based on sagnac loop and I/Q detection," *IEEE Trans. Instrum. Meas.*, vol. 70, 2021, Art no. 5500809.

[19] K. Zhang *et al.*, "Photonic approach to wideband Doppler frequency shift estimation system based on a DPMZM and a Sagnac loop," *Optik*, vol. 182, pp. 219–226, 2019.

[20] Y. Yang, C. Du, D. Wang, M. Wang, and W. Dong, "Simple Doppler frequency shift measurement scheme based on microwave photonics," *IEEE Photon. Technol. Lett.*, vol. 34, no. 1, pp. 67–70, Jan. 2022.

[21] Z. Tu, A. Wen, Z. Xiu, W. Zhang, and M. Chen, "Angle-of-arrival estimation of broadband microwave signals based on microwave photonic filtering," *IEEE Photon. J.,* vol. 9, no. 5, Oct. 2017, Art no. 5503208.

[22] W. Beardell, G. Schneider, J. Murakowski, and D. Prather, "Progress toward instantaneous microwave photonic spatial-spectral localization," in *Proc. SPIE*, vol. 12000, pp. 48–56, 2022 .

[23] R. K. Mohan, C. Harrington, T. Sharpe, Z. W. Barber, and W. R. Babbitt, "Broadband multi-emitter signal analysis and direction finding using a dual-port interferometric photonic spectrum analyzer based on spatial-spectral materials," in *Proc. Int. Topics Meeting Microw. Photon.*, 2013, pp. 241–244.

[24] E. Nova, J. Romeu, S. Capdevila, F. Torres, and L. Jofre, "Optical signal processor for millimeter-wave interferometric radiometry," *IEEE Trans. Geosci. Remote Sens.*, vol. 52, no. 5, pp. 2357–2368, May 2014.

[25] H. Zhuo, A. Wen, and Y. Wang, "Photonic angle-of-arrival measurement without direction ambiguity based on a dual-parallel Mach–Zehnder modulator," *Opt. Commun.*, vol. 451, pp. 286–289, 2019.

[26] P. Li *et al.*, "Photonic approach for simultaneous measurements of Doppler-frequency-shift and angle-of-arrival of microwave signals," *Opt. Exp.*, vol. 27, no. 6, pp. 8709–8716, 2019.

[27] C. Huang, H. Chen, and E. H. W. Chan, "Simple photonics-based system for Doppler frequency shift and angle of arrival measurement," *Opt. Exp.*, vol. 28, no. 9, pp. 14028–14037, 2020.

[28] J. Zhao, Z. Tang, and S. Pan, "Photonic approach for simultaneous measurement of microwave DFS and AOA," *Appl. Opt.*, vol. 60, no. 16, pp. 4622–4626, 2021.

[29] M. Han *et al.*, "Linearity improvement of analog photonic link based on a phase-coherent orthogonal light wave generator," *Opt. Lett.*, vol. 46, no. 15, pp. 3753–3756, 2021.

[30] J. T. Placienre Jr., B. B. Dingel, and F. S. R Borja, "Compensation technique against back-reflected signals in minimalist-designed linear frequency discriminator for microwave photonic links," in *Metro and Data Center Optical Networks and Short-Reach Links*. vol. 12027. Bellingham, Washington, USA: SPIE, 2022, pp. 123–131.